The Structure of a Zn(II) Metaphosphate Glass. I. The Cation Coordination by a Combination of X-Ray and Neutron Diffraction, EXAFS and X-Ray Anomalous Scattering

M. Bionducci, G. Licheri, A. Musinu, G. Navarra, G. Piccaluga, and G. Pinna
Dipartimento di Scienze Chimiche, Via Ospedale 72, 09124 Cagliari, Italy

Z. Naturforsch. **51 a,** 1209–1215 (1996); received September 17, 1996

In order to clarify the reason of some discrepancies existing in literature, the zinc coordination in a Zn metaphosphate glass has been investigated by the complementary use of X-Ray Diffraction, Neutron Diffraction, Extended X-ray Absorption Fine Structure Spectroscopy and X-Ray Anomalous Scattering. All the techniques indicate a tetrahedral coordination of O atoms around Zn^{2+} ions, the Zn-O distance being 1.94 ± 0.01 Å. The simultaneous modelling of all the experimental data by Reverse Monte Carlo technique demonstrated that this coordination is consistent with an extended model in which metal ions are interposed between phosphate chains. The importance of describing the preparation conditions of the glasses is stressed when structural results have to be compared.

Key words: Glass, structure.

1. Introduction

From a structural point of view, glasses are defined as amorphous solids without periodicity in the arrangement of atoms and long range order. However, short range order is present and is responsible for the structural behaviour and physical properties. For instance, the structure of all metaphosphate glasses is described as consisting of long chains of PO_4 tetrahedra, interconnected by bridging oxygen atoms [1, 2]. Differences among the various metaphosphates arise from the different short-range order around the cations that link together the adjacent poliphosphate chains. For this reason the studies about short range order in glasses have been flourishing in recent years and new experimental techniques have been made available.

Unfortunately, the information obtained is still lacunar, and discrepant results are often found in the literature. For instance, zinc metaphosphate glasses have been investigated by many groups because of their interesting physical properties (chemical and mechanical stability, luminescent or semiconductive properties obtained by doping). In these studies [3 - 9] considerable uncertainties exist about Zn coordination; this can be seen in Table 1, where the different results are reported together with the indication of the investigative technique used.

Table 1. Zn^{2+} coordination parameters (mean distance, r, and coordination number, N), density, d, and preparation conditions of zinc metaphosphate glasses.

Reference	r_{Zn-O} (Å)	N_{Zn-O}	d (g/cm^3)	Starting Materials	Melting temp. (K)	Technique
Matsubara *et al.* [3]	1.95	4.0	—	$Zn_3(PO_4)_2$, H_3PO_4	1623 - 1673	XRD
Matz *et al.* [4]	1.92	3.75	2.850	ZnO, H_3PO_4	1475	ND
Musinu *et al.* [5]	2.00	5.0	3.090	$Zn_3(PO_4)_2$, H_3PO_4	1525	XRD
Matsubara	1.96	4.9	—	$Zn_3(PO_4)_2$,	1623 - 1673	XRD
et al. [6]	1.97	4.7	—	H_3PO_4		XAS
Hoppe *et al.* [7]	1.96	4.1	2.85	ZnO, H_3PO_4	1475	XRD
Musinu *et al.* [8]	2.00	4.7	3.090	$Zn_3(PO_4)_2$, H_3PO_4	1525	XRD
Hoppe	1.95	4.0	2.85	ZnO,	1475	XRD
et al. [9]	2.40	0.5		H_3PO_4		and ND

Obviously, these disagreements may arise from systematic errors during the collection and treatment of the different type of data and/or from different assumptions made during the interpretation procedures. This is likely to be true when new, not yet standard techniques are used. However, real differences in the samples examined have not to be underestimated.

Reprint requests to Prof. Giorgio Piccaluga,
Fax: +39 70 6758605.

0932-0784 / 96 / 1200-1209 $ 06.00 © – Verlag der Zeitschrift für Naturforschung, D-72072 Tübingen

In fact, vitreous materials are not in thermodynamic equilibrium and their structure and properties may depend on the preparation route. In this connection, it has to be stressed that the samples used in the investigations mentioned in Table 1 differ either in their precursor compounds or in the melting temperature and consequently in the quenching rate. Different densities may result and can be explained on the basis of differences in coordination numbers, which heavily affect the molar volumes [10]. A clear example of this are the values of density and coordination number proposed by Musinu at al. [5, 8], which are the highest ones reported in Table 1.

It is therefore important to ascertain the part of disagreement coming from the experiments and the one arising from real differences in the samples. To this end it is necessary to investigate by different techniques samples prepared exactly in the same way and, as a consequence, having identical structure. The present study reports the results obtained by X-ray diffraction (XRD), neutron diffraction (ND), extended X-ray absorption fine structure spectroscopy (EXAFS) and X-ray anomalous scattering (XAS) on samples of vitreous zinc metaphosphate prepared in the same laboratory under identical conditions.

2. Experimental

Reagent grade ZnO (Jannsen) and H_3PO_4 (Carlo Erba RPE) were used as starting materials. Weighed amounts of the appropriate mixtures were melted at 1523 K for 2 h in an alumina crucible and then poured into a stainless steel mould and annealed for 2 h at 573 K.

A possible loss of P_2O_5 at the working temperature was checked by weighing the cooled melt; no significant deviations of the weight from the expected value were observed. The density, measured by the immersion method using methanol as immersion liquid, turned out to be 2.795 g/cm^3.

As a further check of the glass composition, ^{31}P MAS-NMR experiments were performed on a Brucker Unity DSX 300 operating at 121.4 MHz. The spectra were recorded at room temperature and spinning rate of 15 KHz. ^{31}P chemical shifts were expressed in ppm relative to 85% H_3PO_4 solution. In Fig. 1 the ^{31}P MAS-NMR spectrum is reported. It shows a band with a chemical shift value typical of PO_4 middle units, with only a very small signal in the region of end groups. This result is in very good agreement with that reported for Zn phosphate glasses at the metaphosphate composition [11].

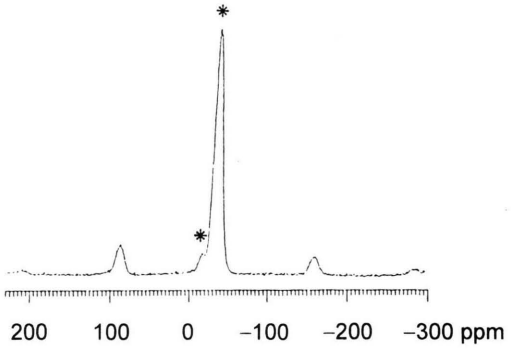

Fig. 1. ^{31}P MAS-NMR spectra. The isotropic chemical shifts are marked with asterisks, the remaining peaks are spinning sidebands.

The surface of the sample, obtained in form of a square slab 2×2 cm and 0.5 cm thick, was polished for the XRD and XAS measurements; powdered samples were used for EXAFS and ND measurements. Data collection and treatment procedures are described in detail in [5, 8, 12 - 14]; only the essential information is reported in the following.

X-ray diffraction data were collected, with MoKα radiation ($\lambda = 0.709$ Å), using a Siemens θ - 2θ diffractometer equipped with a graphite monochromator in the diffracted beam. At least 100,000 counts were collected with a scanning step of $\Delta\theta = 0.25°$ in the angular range $2° < \theta < 30°$, and at least 200,000 counts in the range $30.5° < \theta < 68°$ with a scanning step of $\Delta\theta = 0.5°$. The observed intensities were corrected for background, absorption and polarization, and normalized by a semiempirical method [5, 8].

Neutron scattering measurements were performed on the 7C2 spectrometer located on the hot source of the reactor Orphee (Saclay, Paris) [12]. Diffraction data were collected by a 640-cell position sensitive detector covering an angular range of 128° in steps of 0.2° using a 0.705 Å wavelength (Cu111 Bragg reflection). A huge vacuum vessel both ensures a low background and the absence of hydrogen contamination around the sample. Neutron scattering data were treated using standard procedures, which include subtraction of cell intensities, absorption and multiple scattering corrections and normalization with a vanadium standard [12].

In a disordered multicomponent system, where m atomic species are present, the measured X-ray or

neutron intensities are related to the total structure function (TSF) $i(s)$, where $s = 4\pi(\sin\theta)/\lambda$, is the modulus of the scattering vector, 2θ is the scattering angle and λ the photon wavelength. In the Faber-Ziman formalism, $i(s)$ can be written as a weighted sum of m(m+1)/2 partial structure factors $i_{\alpha\beta}(s)$:

$$i(s) = \sum_{\alpha\beta} w_{\alpha\beta}\, i_{\alpha\beta}(s) \qquad (1)$$

where $w_{\alpha\beta}$ for X-ray is defined as

$$w_{\alpha\beta} = c_\alpha\, c_\beta f_\alpha(s,E) f_\beta(s,E) \,/\, |\langle f(s,E)\rangle|^2. \qquad (2)$$

E is the photon energy and c_α the concentration of the species α. The atomic scattering amplitudes with the real and imaginary part of dispersion corrections, $f(s,E)$, and their average, in (2) are defined as

$$f(s,E) = f_0(s) + f'(s,E) + f''(s,E);$$
$$|\langle f\rangle|^2 = |\sum_\alpha c_\alpha f_\alpha|^2. \qquad (3)$$

The dependence of f' and f'' on the scattering angle is negligible, but they change abruptly when the energy of the incident beam is tuned near one absorption edge of the species α.

For neutron diffraction the terms f_α, in (3), must be substituted by the corresponding energy and angle independent scattering amplitudes b_α.

From the total structure functions, the correlation functions were evaluated by Fourier transform:

$$g(r) = 1 + \frac{1}{2\pi^2 r\rho}\int_{s_{\min}}^{s_{\max}} s(i(s) - 1)\sin(sr)\, M(s)\, \mathrm{d}s, \qquad (4)$$

where r is the interatomic distance and ρ the mean atomic number density. $M(s)$ is a modification function [5, 8, 12, 15] which may include a damping factor, $\exp(-bs^2)$. No correction for spurious ripples was applied.

The value of $s_{\max}$ used for the calculation of the Fourier transform was $\sim$16.0 Å^{-1} for both X-rays and neutron experiments.

XAS technique allows to get the differential structure function, describing the structure around atom A (DSF_A). It can be obtained by performing scattering experiments at two energies, respectively near and far from an absorption edge of the element A. By taking the differences between these two data sets, all terms not involving the chosen atom disappear, since the atomic scattering factors for other species are, to a good approximation, constant at the two energies used. The X-ray diffraction data for XAS analysis were collected at the Lure (Orsay, France) using the DCI synchrotron radiation source [14, 15]. The sample was placed in a vacuum chamber to avoid any air scattering contribution to the measured signal. The experimental apparatus consists of a two circle diffractometer equipped with a Solid State multidetector comprising 12 Si:Li detectors. With this apparatus, the time needed to obtain a good signal/noise ratio was reduced.

Table 2. Anomalous scattering factors (electrons) calculated at the different energy values.

		Zn		P		O	
	eV	f'	f''	f'	f''	f'	f''
E_1	9.654	-8.118	.641	.229	.306	.031	.022
E_2	9.552	-4.773	.492	.230	.310	.032	.023
E_3	19.200	.233	1.209	.064	.077	.010	.005

Three photon energies, reported in Table 2 with the corresponding values of f' and f'', have been suitably chosen to yield significant changes in the real part, f', of the Zn anomalous scattering factor. The energy E_1, very close to the K-edge of Zn, has been selected below the edge in order to reduce the emission fluorescence. The energy E_2 is far enough from the edge to yield a significant variation in f' but not too far, in order to take advantage of the cancellation of systematic errors in calculating DSF_A. The energy resolution of the multidetector is sufficient to resolve the K_α but not the K_β fluorescence from the elastic signals at the energies closer to the K edges. For this reason the energy E_3 has been chosen far from the K-Zn edge, to evaluate the experimental ratio K_α/K_β.

The EXAFS experiment was carried out in air at room temperature, at the EXAFS-I station mounted on DCI (1.85 GeV, about 250 mA) storage ring, at LURE, Orsay, using a channel cut monochromator Si (311) and two ionization chambers filled with air [13]. The spectral range 9500 - 10500 eV (ΔE = 2 eV) was scanned for Zn K-edge. Each point was measured for 1.5 s and the spectral range was scanned three times. The EXAFS data processing was carried out using standard procedures which are briefly summarized. The background contribution, originating from the pre-edge region, was extrapolated using the Victoreen relationship, and then subtracted from the experimental data. The smooth atom-like contribution, $\mu_0(k)$, was obtained by cubic splines. The edge energy, E_0, was arbitrarily chosen at the edge inflection.

The EXAFS function

$$\chi(k) = \frac{\mu(k) - \mu_0(k)}{\mu_0(k)}, \qquad (5)$$

multiplied by a k^3 factor, was Fourier transformed in the range of the photoelectron wavevector k = 3.2 - 15.2 Å^{-1} ($k = [(E - E_0)^2\, m/\hbar^2]^{1/2}$) after application of a Hanning window.

3. Results

Figures show the radial functions obtained from:

a) in home X-ray diffraction data (Fig. 2);

b) neutron diffraction data (Fig. 3);

c) EXAFS data (Fig. 4);

d) single X-ray diffraction experiment by synchrotron radiation (Fig.5);

e) difference diffraction data from X-ray anomalous scattering experiments (Figure 6).

The curves of Figs. 2, 3 and 5 represent total radial functions. The shortest Zn-O distance gives rise to the peak centred at about 1.95 Å, partially superimposed to the P-O peak at about 1.55 Å on the left and to the O-O peak at about 2.5 Å on the right. It is more prominent in the X-ray diffraction results because, according to (2), the weight of the Zn-O term is greater in the X-ray experiment than in the neutron one. The weights of the three terms mentioned above are reported in Table 3.

Table 3. Weighting factors for XRD (calculated at $2\theta = 0$) and ND for the different pairs in $Zn(PO_3)_2$.

	Zn-Zn	P-P	O-O	Zn-P	Zn-O	P-O
XRD	0.077	0.077	0.199	0.155	0.248	0.249
ND	0.013	0.041	0.471	0.045	0.154	0.277

The peaks in the curves in Fig. 4 and Fig. 6 correspond to the distances between Zn and the surrounding atoms. In the EXAFS radial function the peaks are shifted from the true values because of the k-dependence of the phase shift in the sine argument of the EXAFS equation [13, 15]. Besides, higher r peaks in EXAFS radial curve are less important because the signals from shells beyond the first are more quickly dampened in EXAFS than in XRD. A further difference in the results follows from the different ranges of scattering vectors explored in the various experiments, which affect the resolution of the radial curves.

The coordination of Zn atoms was evaluated by fitting procedures described in detail elsewhere [5, 8, 12 - 15]. In diffraction experiments these procedures are based on the Debye scattering equation, which describes the structure function as a sum of contributions from each atom pair distance in the system

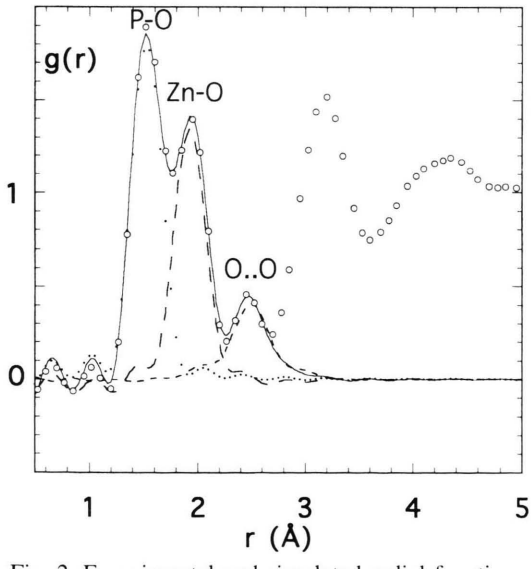

Fig. 2. Experimental and simulated radial functions, from in house X-ray diffraction data, calculated with a damping factor b = 0.005.

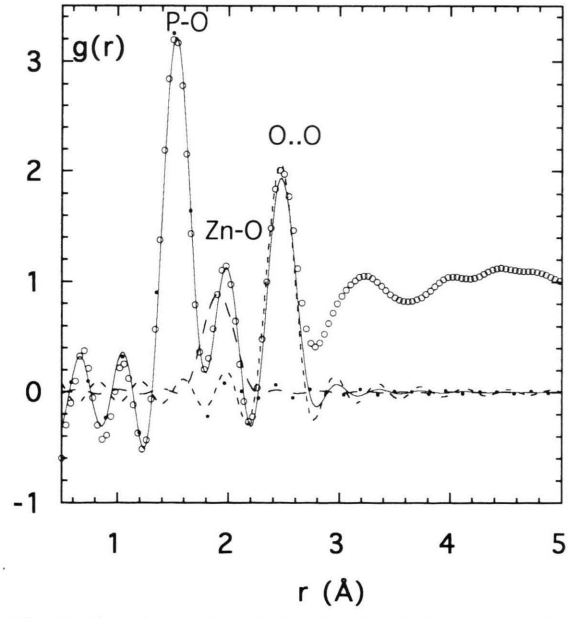

Fig. 3. Experimental and simulated radial functions from neutron diffraction data.

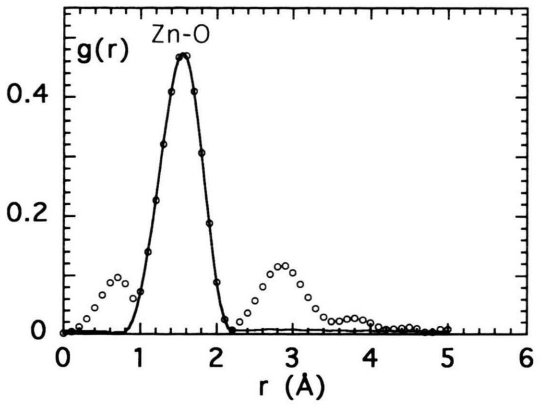

Fig. 4. Experimental and simulated radial functions from EXAFS data.

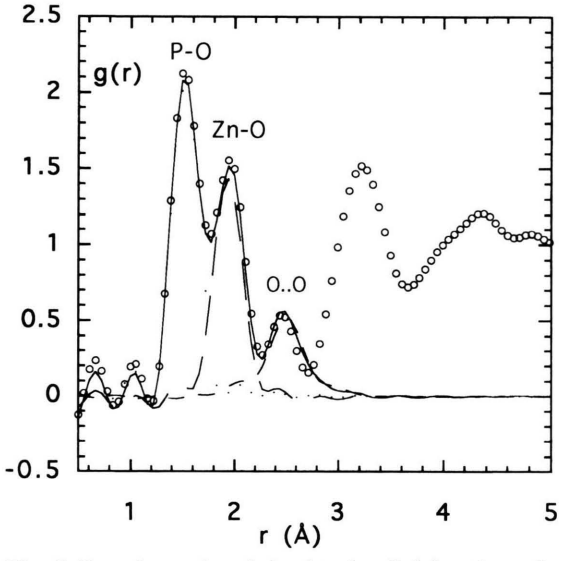

Fig. 5. Experimental and simulated radial functions, from single X-ray diffraction experiment by synchrotron radiation, calculated with a damping factor $b = 0.005$.

[15]. When the study is limited to the evaluation of the short range order, it is usual to simulate low r peaks in the radial functions by Fourier transforming the proper terms of the Debye equation; the agreement between experimental and synthetic peaks is optimized by varying the physical parameters r_{ij} (interatomic distance), N_{ij} (coordination number) and σ_{ij} (root mean square deviation of r_{ij}). Alternatively, the fitting can be performed in the reciprocal space. This is the most common procedure in EXAFS data analysis, which, in addition, requires the investigation of

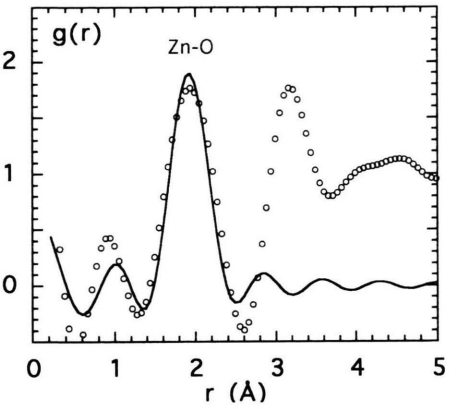

Fig. 6. Experimental and simulated radial functions from differential X-ray anomalous scattering data.

some standard compound to determine phase shifts and backscattering amplitudes of the species investigated [13]. In the present case, ZnO was used as reference sample. In any case the results of the fitting calculations can be visualized in the real space; Figures 2 - 6 show as a solid line the radial curves from the best fittings.

4. Discussion

Final parameters from the best fits of the experimental results are reported in Table 4. When total radial functions are interpreted, P-O and O-O peaks are simulated together with the Zn-O one and the related parameters are also reported in the Table 4. In these cases, the determination of the Zn coordination parameters can be hampered by the partial overlapping of the three main peaks of the radial curves. However, the P-O peaks can be used to check the correctness of the experimental and interpretation procedures; in fact, deviations of the P-O structural parameters from the values expected for P tetra coordination are a direct proof of errors or approximations. In the present case, the parameters values reported in Table 4 point out a substantial correctness of all the experiments.

The picture of the structural parameters for Zn-O interactions is as much satisfactory. Five independent fittings provide results in very good agreement, despite the different nature of the experiments, the different weight and resolution of the Zn-O term in the various radial curves, the different fitting procedures. As usual, the distance is determined with the greatest precision; according to the ionic radii given by Shannon and Prewitt [16], it points a tetrahedral

Table 4. Structural parameters from the best fits and Reverse Monte Carlo calculations.

	XRD home	ND	EXAFS	XRD Synch.	XAS	RMC
r_{P-O}	1.53(1)	1.53(1)		1.53(1)		1.52
σ_{P-O}	0.07(1)	0.06(1)		0.07(1)		
N_{P-O}	3.8(2)	4.0(1)		4.0(2)		4.0
r_{Zn-O}	1.94(1)	1.93(1)	1.94(1)	1.95(1)	1.94(1)	1.94
σ_{Zn-O}	0.10(1)	0.12(2)	0.08(2)	0.08(1)	0.08(1)	
N_{Zn-O}	3.9(3)	4.0(2)	3.7(3)	4.1(2)	4.1(3)	3.8
r_{O-O}	2.50(1)	2.47(1)		2.51(1)		2.48
σ_{O-O}	0.11(1)	0.07(2)		0.09(2)		
N_{O-O}	4.1(3)	3.8(3)		4.5(3)		4.5

coordination of Zn^{2+}, which is well confirmed by the coordination number values.

A slightly higher uncertainty affects the parameters describing O-O interactions. This is not surprising, because the O-O peak is not resolved on its right side and the fittings are strongly conditioned by higher distance distributions. In the light of this consideration, further fittings were performed with the aim of simulating the medium range order of the radial (and structure) functions through the use of extended structural models.

Reverse Monte Carlo technique was used to optimize the agreement between experimental and model radial functions [17 - 18]. All the experimental curves were simultaneously modelled. This means that the differences between each experimental structure function and the one calculated from a configuration of atomic positions were summed and minimized. The resulting "best" structural configuration is consistent with all the experimental data. Details of the construction of the starting model and of the fitting procedures will be reported elsewhere [19]. Here we wish to underline that good simulations were obtained, where Zn^{2+} coordination from the analysis of the first peaks of the radial curves, turned out consistent with an extended model in which Zn^{2+} ions are interposed between phosphate chains. Structural parameters from Reverse Monte Carlo calculations are reported in Table 4.

5. Conclusions

The zinc coordination in a Zn metaphosphate glass has been investigated by X-ray diffraction, neutron diffraction, EXAFS spectroscopy and X-ray anomalous scattering experiments. All the investigations came to the conclusion that Zn^{2+} ions are tetracoordinated with O atoms, the distance Zn-O being 1.94 ± 0.01 Å.

The simultaneous modelling of all the experimental data by Reverse Monte Carlo techniques demonstrated that this coordination is consistent with an extended model in which metal ions are interposed between phosphate chains.

These results suggest that the discrepancies existing in literature about the Zn coordination in $Zn(PO_3)_2$ glasses mainly stem from real differences in the structure of the glasses investigated. In the light of the non-equilibrium status of vitreous materials this conclusion is not surprising.

Great caution has to be used when comparisons of different structural investigations are made. In fact, they are meaningful only if the chemical composition, density and thermal history of the different samples are rigorously the same; obviously, details about these data should not be lacking in the published papers.

Acknowledgements

Measurements have been performed on samples kindly provided by Prof. M. Bettinelli (Universita' di Verona, Italy). This work has been supported by Regione Sardegna, MURST, CNR (Italy) and European Community (Contract N° 920001).

[1] J. R. Van Wazer, Phosphorus and Its Compounds, Interscience, New York 1951.

[2] S. W.Martin, Eur. J. Solid State Inorg. **28**, 163 (1991) and Ref. therein quoted.

[3] E. Matsubara, Y. Waseda, M. Ashizuka, and E. Ishida, J. Non-Crystalline Solids **103**, 117 (1988).

[4] W.Matz., D. Stachel, and E. A. Goremychkin, J. of Non-Crystalline Solids **101**, 80 (1988).

[5] A. Musinu, G. Piccaluga, G. Pinna, D. Narducci, and S. Pizzini, J. Non-Crystalline. Solids **111**, 221 (1989).

[6] E. Matsubara, K. Sugiyama, Y. Waseda, M. Ashizuka, and E. Ishida, J. Mat. Sci. Lett. **9**, 14 (1990).

[7] U. Hoppe, G. Walter, and D. Stachel, Phys. Chem Glasses **33**, 216 (1992).

[8] A. Musinu, G. Paschina, G. Piccaluga, and G. Pinna, J. Non-Crystalline Solids **177**, 97 (1994).

[9] U. Hoppe, D. Stachel and D. Beyer, Physica Scripta **1995**, T57, 122.
[10] R. K. Brow, D. R. Tallant, S. T. Myers and C. C. Phifer, J. Non-Crystalline Solids **191**, 45 (1995).
[11] R. J. Kirkpatric and R. K. Brow, Solid State NMR, 9 (1995).
[12] M. Bionducci, R. Bellissent, M. P. Medda, G. Piccaluga, G. Pinna, and M. Bettinelli, J. Non-Crystalline Solids **192&193**, 36 (1995).
[13] G. Navarra, M. Bionducci, and G. Licheri, to be published in the proceedings of EXAFS IV Intern. Conf., Grenoble 1996, J. de Physique IV, Colloques.
[14] G. Navarra, M. Bionducci, G. Licheri and B. Bouchet-Fabre, in preparation. G. Navarra, M. Bionducci, F. Buffa, and G. Licheri, Methods in the Determination of Partial Structure Factors, edited by J. B. Suck, D. Raoux, P. Chieux, C. Riekel, World Scientific 155 (1993).
[15] M. Magini, G. Licheri, G. Paschina, G. Piccaluga, and G. Pinna, X-Ray Diffraction of Ions in Aqueous Solutions, edited by M. Magini, CRC Press, Boca Raton, Florida 1988.
[16] R.D. Shannon and L.T. Prewitt, Acta Crystallogr. **B25**, 925 (1969).
[17] R. L. Mc Greevy and L. Pustzai, Molec. Simul. **1**, 359 (1988).
[18] R. L. Mc Greevy and M. A. Howe, Ann. Rev. Mater. Sci. **22**, 217 (1992).
[19] G. Navarra, M. Bionducci, and G. Licheri, in preparation.